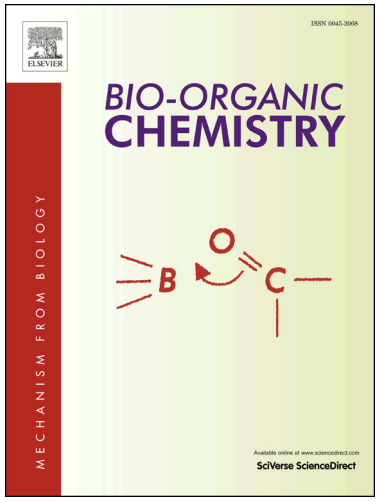

Anticancer and structure-activity relationship evaluation of 3-(naphthalen-2-yl)-*N*,5-diphenyl-pyrazoline-1-carbothioamide analogs of chalcone

Youngshim Lee, Beom Soo Kim, Seunghyun Ahn, Dongsoo Koh, Young Han Lee, Soon Young Shin, Yoongho Lim

PII: S0045-2068(16)30089-X
DOI: http://dx.doi.org/10.1016/j.bioorg.2016.08.003
Reference: YBIOO 1937

To appear in: *Bioorganic Chemistry*

Received Date: 20 June 2016
Revised Date: 3 August 2016
Accepted Date: 4 August 2016

Please cite this article as: Y. Lee, B.S. Kim, S. Ahn, D. Koh, Y.H. Lee, S.Y. Shin, Y. Lim, Anticancer and structure-activity relationship evaluation of 3-(naphthalen-2-yl)-*N*,5-diphenyl-pyrazoline-1-carbothioamide analogs of chalcone, *Bioorganic Chemistry* (2016), doi: http://dx.doi.org/10.1016/j.bioorg.2016.08.003

Anticancer and structure-activity relationship evaluation of 3-(naphthalen-2-yl)-*N*,5-diphenyl-pyrazoline-1-carbothioamide analogs of chalcone

Youngshim Lee[a,+], Beom Soo Kim[a,+], Seunghyun Ahn[a], Dongsoo Koh[b], Young Han Lee[c], Soon Young Shin[c,*], and Yoongho Lim[a,*]

[a]*Division of Bioscience and Biotechnology, BMIC, Konkuk University, Seoul 143-701, Korea*
[b]*Department of Applied Chemistry, Dongduk Women's University, Seoul 136-714, Korea*
[c]*Department of Biological Sciences, Konkuk University, Seoul 143-701, Korea*

[+]These authors contributed equally to this work.

*__Corresponding authors__:
Prof. Yoongho Lim; Division of Bioscience and Biotechnology, Konkuk University
Hwayang-Dong 1, Kwangjin-Ku, Seoul, Korea 143-701
Tel.: 82-2-450-3760; Fax: 82-2-3437-6106; Email: yoongho@konkuk.ac.kr

Prof. Soon Young Shin; Department of Biological Sciences, Konkuk University
Hwayang-Dong 1, Kwangjin-Ku, Seoul, Korea 143-701
Tel.: 82-2-2030-7946; Fax: 82-2-3437-9781; Email: shinsy@konkuk.ac.kr

Abbreviations: CoMFA, comparative molecular field analysis; CoMSIA, comparative molecular similarity index analysis; GI_{50}, half-maximal cell growth inhibitory concentration NDPC, 3-(naphthalen-2-yl)-*N*,5-diphenyl-pyrazoline-1-carbothioamide

Abstract

To identify new potent chemotherapeutic agents, we synthesized compounds with 3-(naphthalen-2-yl)-*N*,5-diphenyl-pyrazoline-1-carbothioamide (NDPC) skeletons and evaluated their cytotoxicities using a clonogenic long-term survival assay. Their half-maximal cell growth inhibitory concentrations ranged from a few hundred nanomolars to a few micromolars. Further biological experiments including flow cytometry and western blotting analysis were performed with the derivative showing the best cytotoxicity. To identify a target protein of the selected compound, an *in vitro* kinase assay was carried out, which revealed that aurora kinases A and B were inhibited by the test compound, and this was confirmed using western blot analysis. The molecular binding mode between the selected compound and the kinases was elucidated using *in silico* docking. The structural conditions required for good cytotoxicity were identified based on the quantitative relationships between the physicochemical properties of the derivatives and their cytotoxicities.

Keywords: colorectal, clonogenicity, QSAR, flow cytometry, immunofluorescence microscopy, *in silico* docking

1. Introduction

Compounds containing pyrazoline-1-carbothioamide moiety show antidepressant and anticonvulsant activities [1], as well as pesticide activities against the yellow fever mosquito vector (*Aedes aegypti*) [2]. However, their anticancer activities have been rarely reported. Compounds containing diphenylpyrazoline moiety show anticancer activities [3]. To identify compounds with potential for use as chemotherapeutic agents, we combined the structures of pyrazoline-1-carbothioamide and diphenylpyrazoline to create diphenylpyrazoline-1-carbothioamide (Figure 1A). It has been reported diphenylpyrazoline-1-carbothioamide derivatives show anticonvulsant and antidepressant activities [1]. Furthermore, to obtain asymmetrical structures, one phenyl ring of the compound was switched with naphthalene. Since the methoxylation of polyphenols can enhance cell permeability and stability [4], methoxylated derivatives were designed (Figure 1B).

Colorectal cancer is one of the most common types of cancer in both developing and advanced countries. Most colorectal cancers begin as a polyp in the inner lining of the large intestine and over 90% occurred in gland cells lining the inside of the colon and rectum. The exact causes of colorectal cancer are not known exactly, but some risk factors have been identified including a high-fat diet, family history, genetic mutations, age, smoking, and ulcerative colitis. Several studies have demonstrated that numerous bioactive polyphenols have chemopreventive or therapeutic effects against colon cancer cells [5].

Because cancer cells divide faster than normal cells do, a cytotoxicity test can be a screening tool to measure the anticancer activities of compounds. The compounds synthesized in this study have the same basic 3-(naphthalen-2-yl)-*N*,5-diphenyl-pyrazoline-1-carbothioamide (NDPC) skeleton, and differ only in except the methoxy groups (Figure 1C). In addition, it was found that hydroxylation of naphthalenyl group increased the inhibitory effect on aurora kinases [3], so that 1-hydroxy group was added to naphthalenyl group (Figure 1D). To distinguish the cytotoxicities of the synthesized compounds, a clonogenic long-term survival assay was used because the result, which is obtainable after 7 days, can clarify the distinction between similar structures [6]. Here, 36 compounds containing NDPC skeletons were synthesized, and their colonogenicities were

tested. In addition, further biological experiments including flow cytometry and western blotting analysis were performed to elucidate the cytotoxicities of the compounds. Furthermore, to identify the target protein of the compounds, an *in vitro* kinase assay was carried out based on the superior half-maximal cell growth inhibitory concentration (GI_{50}) exhibited by the selected compound in inhibiting these kinases. The molecular binding mode between the selected compound and the kinases was also elucidated using *in silico* docking. Moreover, the structural conditions required for good cytotoxicity were determined based on the evaluation of the quantitative relationships between the physicochemical properties of the compounds and their cytotoxicities.

2. Materials and Methods

2.1. Preparation of NDPC derivatives

All the compounds (**1**–**36**) containing the NDPC skeleton were synthesized using previously reported methods [7,8]. Synthetic procedures are shown in Scheme 1 where the intermediate chalcone **III** was obtained from Claisen-Schmidt condensation reaction between 1'-hydroxy-2'-acetonaphthone **I** and methoxy-substituted benzaldehyde **II**. Chalcone **III** was treated with excess amount of hydrazine to give pyrazoline **IV**, which was reacted with isothiocyanate in ethanol to furnish desired compounds NDPC **1-36**. After recrystallization, analytically pure compounds of NDPC **1-36** were obtained. Their chemical identification was performed by analyzing basic one- and two-dimensional (1D and 2D, respectively) nuclear magnetic resonance (NMR) spectroscopy and high-resolution electron impact ionization mass spectrometry (MS) spectra as reported previously [7,8]. All the NDPC derivatives prepared here are novel, and their structures are listed in Table 1. Their melting points were measured using a Mel-Temp II melting point apparatus (LabX, Midland, ON, Canada) and were uncorrected while the infrared (IR) spectra were acquired using a Fourier transform (FT)-IR 4200 (JASCO, Easton, MD, USA) with attenuated total reflection (ATR, PR0450-S). The column chromatography purifications were performed on Silica gel 60 (70−230-mesh, Merck, Whitehouse Station, NJ, USA) when it was necessary [9]. The chemical data including names, colors, melting points, yields, IR, NMR, and

HRMS were determined completely as provided in Supplementary materials [7,8].

2.2. Clonogenic assay

The HCT116 human colorectal cancer cells were obtained from the American Type Culture Collection (ATCC, Rockville, MD, USA) and were grown in Dulbecco's modified Eagle's medium (DMEM, Invitrogen Life Technologies, Carlsbad, CA, USA) supplemented with 10% (v/v) heat-inactivated fetal bovine serum (FBS, HyClone, Logan, UT, USA). For the experiment, the HCT116 cells (3×10^3 cells/well) were seeded in 24-well tissue culture plates (BD Falcon, Franklin Lakes, NJ, USA) in the absence or presence of different concentrations of the 36 compounds, incubated for 7 days, and were tested on four plates treated with 0, 5, 10, and 20 μM of the samples. The colorectalies that formed were fixed with 6% glutaraldehyde and stained with 0.1% crystal violet as described previously [6]. Since most of the compounds containing the NDPC skeleton inhibited the cancer cell lines completely, the clonogenic long-term survival assays were repeated using lower concentrations (0, 50, 500, and 5000 nM). The results of the clonogenic survival assay were analyzed using densitometry (MultiGuage, Fujifilm, Japan). The GI_{50} values were determined using the SigmaPlot software (SYSTAT, Chicago, IL, USA) and their negative logarithmic scales (pGI_{50}) were considered as the biological data of each NDPC compound (Table 1) [10].

2.3. Quantitative structure–activity relationship (QSAR)

The quantitative structure-activity relationship (QSAR) calculations were carried out using an Intel Core 2 Quad Q6600 (2.4 GHz) Linux PC with the Sybyl 7.3 software (Tripos, St. Louis, MO, USA) using comparative molecular field analysis (CoMFA) and comparative molecular similarity index analysis (CoMSIA) [11]. The previously unknown 3D structures of all the NDPC derivatives needed to be determined, and the 3D structure of *N*,3,5-triphenyl-pyrazoline-1-carbothioamide (Suppl. Figure 1) obtained from National Center for Biotechnology Information (NCBI, PubChem CID: 3794935) was used as a template for the determination. The 3D structures constructed based on *N*,3,5-triphenyl-pyrazoline-1-carbothioamide were subjected to energy minimization using the molecular mechanic algorithms provided by Sybyl 7.3 [3]. The

compounds that conformed to the lowest energy were selected for the QSAR calculations. The conformational search to identified the most stable structure, the minimization process, and CoMFA and CoMSIA calculations were performed according to methods reported previously [9].

2.4. Cell cycle and cell death analysis

Flow cytometry was used to assess the cell cycle by measuring the propidium iodide (PI)-stained DNA contents using a NucleoCounter NC-3000 image cytometer (ChemoMetec, Allerød, Denmark) as described previously [12].

2.5. Western blot analysis

The HCT116 cells were treated with 20 μM NDPC compound **4** (**NDPC4**) for different incubation times, harvested, and then lysed in a buffer containing 20 mM 4-(2-hydroxyethyl)-1-piperazineethanesulfonic acid (HEPES, pH 7.2), 1% Triton X-100, 10% glycerol, 150 mM sodium chloride (NaCl), 10 μg/mL leupeptin, and 1 mM phenylmethylsulfonyl fluoride. The total cell lysates containing 10–20 μg protein were separated using sodium dodecyl sulfate-polyacrylamide gel electrophoresis (SDS-PAGE), and transferred to nitrocellulose membranes, which were probed with the primary antibodies of interest. The blots were subsequently incubated with horseradish peroxidase-conjugated secondary antibodies and were visualized using an enhanced chemiluminescence detection system (Amersham Pharmacia Biotech Inc.) [13].

2.6. Kinases assay

We used the following 17 kinases in the cell cycle analysis and *in vitro* kinase assays: aurora kinase A and B (aurA and aurB, respectively), calcium/calmodulin-dependent protein kinase type IV, dual specificity tyrosine-phosphorylation-regulated kinase 2, ephrin type-A receptor 2, haspin Serine/threonine-protein kinase, hepatocyte growth factor receptor, insulin-like growth factor-1 receptor kinase, nuclear factor of kappa light polypeptide gene enhancer in B-cells inhibitor (IκB) kinase α, polo-like kinase 1, protein kinase B, proto-oncogene serine/threonine-protein kinase, serine/threonine-protein kinase PAK 4, TANK-binding kinase 1, transforming growth factor beta-activated kinase-1, tyrosine-protein kinase HCK, and vascular endothelial

growth factor receptor 1. The kinase assay was performed using the EMD Millipore KinaseProfiler service assay protocol (EMD Millipore Corporation, Billerica, MA, USA) [10].

2.7. *In silico* docking

The docking experiments were performed with an Intel Core 2 Quad Q6600 (2.4 GHz) Linux PC with Sybyl 7.3 [14]. The 3D structure of aurA was adapted from 2J4Z.pdb deposited in the protein data bank (PDB) [15] while that of aurB was adapted from 4AF3.pdb [16]. The detailed procedures for *in silico* docking were performed according to previously reported methods [9].

2.8. Statistical analysis

The statistical significance was analyzed using the Student's *t*-test and a $p < 0.05$ was considered statistically significant. All the experiments were performed in triplicate [13].

3. Results and Discussion

3.1. Clonogenic long-term survival assay

As shown in Suppl. Figure 2, the clonogenic assay results obtained with the samples at 0, 5, 10, and 20 µM could not distinguish the activity of the compounds because most of them inhibited the cancer cells completely. Therefore, the GI_{50} values were obtained from the clonogenic long-term survival assays performed at lower different concentrations (0, 50, 500, and 5000 nM, Figure 2). They ranged from 210.55 to 4788.65 nM (NDPC compounds **4** and **3** respectively). The GI_{50} values were obtained using the SIGMAPLOT software (SYSTAT, Chicago, IL), and their negative logarithmic scales (pGI_{50}) were used for the QSAR calculations (Table 1).

3.2. QSAR calculations

The structures of the 36 NDPC derivatives showed slight differences in the position of the methoxy substituents. However, the effects of the compounds on the human colorectal cancer cells vary from 210.55 to 4788.65 nM. To explain why derivatives with similar structures exhibited 22.7 times higher activities than the other derivative did, the QSAR calculations were

performed using an Intel Core 2 Quad Q6600 (2.4 GHz) Linux PC with the Sybyl 7.3 software [11]. Furthermore, CoMFA) and CoMSIA were used for the QSAR calculations. The compounds were divided into two groups, the training and test sets, for the validation of the QSAR model. Seven derivatives (**2**, **9**, **14**, **19**, **24**, **27**, and **35**) were selected randomly as the test set for evaluating the relationship between the structures and cancer cell growth inhibitory activity while other derivatives were used to establish the QSAR model. The derivatives of the test set were analyzed using a hierarchical clustering tree. As shown in Suppl. Figure 3, the seven derivatives that were chosen as the test set belonged to separate structural groups. Therefore, the test set could be used to validate the reliability of the QSAR models used in this experiment.

For the QSAR calculation using CoMFA, a partial least square (PLS) regression was used to elucidate the linear correlation between the calculated fields such as the steric and electrostatic fields and the biological data. The cross-validated correlation coefficient (q^2) and non-cross-validated correlation coefficient (r^2) were calculated based on the overall compounds in the training set. Among the models generated by the CoMFA, the model showing the best cross-validated correlation coefficient ($q^2 = 0.598$) was chosen for the further analysis. The final non-cross-validated ($r^2 = 0.920$) analysis was performed using the optimal number of components (n = 6) obtained using the leave-one-out (LOO) method. In the PLS analysis, the standard error of the estimate was 0.137 and F value was 42.443. To evaluate the CoMFA model, the activities of 36 derivatives were predicted, and their values were compared to the experimental data as shown in Suppl. Table 1. The residuals between the experimental and predicted values for the training set ranged from 0.03% to 10.82%. For the test set, the residuals ranged between 4.04% and 21.78%. The experimental data was plotted against the values predicted by the CoMFA model (Suppl. Figure 4).

To visualize the relationships between the structures of the 36 compounds and their inhibitory activities in the clonogenicity assay, CoMFA contour maps were generated in Suppl. Figure 5. The steric and electrostatic field descriptors contributed 95.5% and 4.5%, respectively. In addition, the only difference between the derivatives was the position of the methoxy substitutions on rings A and B, which can contribute to the steric property considerably, and

therefore, a detailed analysis was conducted on the steric field. The favored steric bulky region was 90%, and the disfavored region was 10%. The electronegative favored region was 90%, and the electropositive region was 10%. As shown in Suppl. Figure 5, a yellow contour observed at the C2 position of the A benzene ring indicates that the absence of a bulky group at C2 is required for the inhibitory activity. All the derivatives that had a methoxy group at C2 showed low inhibition activity such as derivatives **3**, **6**, **9**, **12**, **14**, **17**, **20**, **23,** and **32**. On the other hand, a green contour at C5 position was observed, suggesting that this bulky group at this region increase activity. This was based on the observation of compounds **7**, **13**, **18**, **24,** and **30**. The remaining yellow contours, which were positioned at C2′ and C3′ of the B ring, need a complicated explanation because we assumed that the combination of bulky group substitution is important. For example, compounds dimethoxylated at both meta positions, C3′ and C5′, showed good inhibitory activity supported by NDPC**4**, **15**, **16**, and **18**. Compounds **31**–**36**, which contained tri-methoxy groups at C2′, C4′, and C6′, showed low inhibitory effects. In addition, the derivatives that were dimethoxylated at positions C2′ and C4′ showed better activity than that shown by the derivatives dimethoxylated at C2′ and C3′, when the same substitution was included in the A ring. This observation was based on the comparison of compounds **2** and **11**, **1** and **8**, and **5** and **10**.

Additional information on the QSAR model was obtained by calculating the CoMSIA. Among the numerous CoMSIA models, the best model that showed q^2 and r^2 values of 0.6 and 0.893, respectively. The PLS statistical parameter were the number of components, the standard error of estimate, and the F values, which were 6, 0.159, and 30.543, respectively. To evaluate the CoMSIA model, the activities of the compounds were predicted and compared with that of the experimental data. All the residuals between the experimental and predicted activity values are shown in Suppl. Table 1. For the test set, the residuals between the experimental and predicted values ranged from 2.23% to 23.92%. The residuals for the derivatives in the training set ranged from 0.4% to 11.4%. The experimental data was plotted against the values predicted using the CoMFA model (Suppl. Figure 6) and based on these results, the selected CoMSIA model was determined to be reliable.

In this study, the selected CoMSIA model provided information that the contributions of the steric, electrostatic, hydrophobic, and H-bond acceptor field descriptors were 21.6%, 6.9%, 62.3%, and 9.2%, respectively. The contour maps are shown in Suppl. Figure 7. The steric bulky favored region was 85% while the disfavored region was 15%. The electronegative favored region was 90%, and the electropositive region was 10%. The hydrophobic favored region was 75%, and the disfavored region was 25%. The H-bond acceptor favored region was 8%, and the disfavored region was 92%. Because the information on the steric and electrostatic fields obtained from the CoMSIA maps was similar to that from the CoMFA, the contour maps of the hydrophobic and H-bond acceptor fields were examined. As shown in Suppl. Figure 7 (C), a yellow contour at the C2 position indicates that the hydrophobic substituents at this position increased the inhibitory activity. For examples, the GI_{50} values of derivatives **1** and **19** were better than those of derivatives **3** and **20**. The C2′ position was also associated with the yellow color, which indicates that the methoxy group at that position decreased the activity. Furthermore, derivatives **25**, **27**, and **28** that possess the methoxy group at the C5′ position showed less activity than derivatives **8**, **10**, and **11**, did. The gray contour at position C3 suggests that hydrophilic groups at this positions were favored. This observation is supported by the evidence that derivatives **10**, **13**, **15**, and **18**, which have methoxy groups at this position, showed relatively good inhibitory activity. As shown in Suppl. Figure 7 (D), a purple contour was observed at the hydroxyl group of the naphthalene ring, which was a common structure in all 36 compounds while the cyan contour was not observed in this map. The color of the H-bond acceptor favored and disfavored was cyan and purple, respectively. Therefore, the importance of the H-bond acceptor field was not discovered in this study.

3.3. Evaluation of cellular activities of NDPC4

Next, we evaluated the biological activities of **NDPC4** including its cytotoxicity against HCT116 cells using a cell counting kit-8 (CCK-8). Treatment with **NDPC4** resulted in a concentration-dependent inhibition of the cell viability with an IC_{50} value of ~10 μM (Figure 3A), suggesting that the **NDPC4** exhibited a growth inhibitory effect in cancer cells. To assess whether this decrease in cell viability is associated with inhibition of the cell cycle progression, we analyzed the cell cycle phase distribution using flow cytometry. As shown in Figure 3B, **NDPC4** caused a

considerable decrease in G1 phase cells (from 54% to 29%) with a concomitant increase in S phase cells (from 18% to 35%), whereas the total number of G2/M phase cells was not changed compared with the vehicle-treated control cells. This result suggests that **NDPC4** inhibited cell cycle progression. It is well established that cell cycle progression is regulated by cell cycle regulatory proteins such as cyclin and cyclin-dependent kinase (Cdks) complexes. Among them, cyclin D1 triggers G1 cell cycle progression while cyclin B1 is involved in the regulation of G2/M phase progression. To explore the mechanism underlying the **NDPC4**-induced cell cycle dysregulation, we examined the expression level of cyclin D1 and cyclin B1 using a western blotting assay. We found that treatment of HCT116 cells with 10 μM **NDPC4** remarkably decreased the levels of both cyclin D1 and cyclin B1 in a time-dependent fashion (Figure 3C), suggesting that NDPC compound **4** inhibited the cell cycle progression by downregulating G1 and G2/M cell cycle regulators. Notably, following **NDPC4** treatment at a concentration of 10 μM, the population of sub-G1 cells was increased from 1% (control) to 7% (after treatment), suggesting an induction of apoptosis.

Therefore, we subsequently examined whether **NDPC4** induces apoptosis. It is well established that phosphatidylserine (PS), a membrane phospholipid, is located on the outer membrane of apoptotic cells [17]. Annexin V binds to PS [18] and, therefore, we analyzed annexin V-positive cells (AV^+) after **NDPC4** treatment of cells using flow cytometry. PI was used as a counterstain to detect late apoptotic or necrotic dead cells or both. As shown in Figure 4A, treatment with **NDPC4** decreased the population of viable cells (lower left quadrant, AV and PI double-negative, AV^-PI^-) from 83% to 14% while the early apoptotic cells (lower right quadrant; AV^+PI^-) increased from 13% to 80%. The late apoptotic or dead cells, or both (upper right quadrant; PI^+AV^+) increased from 3% to 6%. Therefore, the total dead cells were increased from 16% to 86% following **NDPC4** treatment (Figure 4B). These data demonstrate that **NDPC4** triggered cell death through apoptosis of HCT116 cells.

Caspases are a family of cysteine-dependent aspartate-directed proteases that play central roles in regulating apoptosis. Caspases are subclassified by their roles as initiator caspases (caspase-9 and -8) and effector caspases (caspase-7 and -3). Following exposure to apoptotic stimuli,

initiator caspases are activated by autocatalytic cleavage. The active initiator caspases then cleave and activate effector caspases, thereby accelerating the cleavage of numerous cellular proteins including the DNA repair enzyme poly(adenosine diphosphate [ADP]-ribose) polymerase (PARP), to induce apoptosis [19]. To explore whether **NDPC4** activates caspases, the HCT116 cells were treated with 20 μM, which is sufficient to induce apoptosis and then the levels of active caspase 7 were determined using a western blotting assay. We found that the cleavage of caspase 7 and its substrate PARP, were increased in response to **NDPC4** treatment (Figure 4C). These results suggest that **NDPC4** induced apoptosis by a caspase-dependent mechanism.

3.4. *In vitro* kinase assay

The *in vitro* kinases assays of **NDPC4** were performed using 17 kinases to evaluate the effects on the cell cycle including aurA, aurB, calcium/calmodulin-dependent protein kinase type IV, dual specificity tyrosine-phosphorylation-regulated kinase 2, ephrin type-A receptor 2, haspin serine/threonine-protein kinase, hepatocyte growth factor receptor, insulin-like growth factor-1 receptor kinase, IκB kinase α, polo-like kinase 1, protein kinase B, proto-oncogene serine/threonine-protein kinase, serine/threonine-protein kinase PAK 4, TANK-binding kinase 1, transforming growth factor beta-activated kinase-1, tyrosine-protein kinase HCK, and vascular endothelial growth factor receptor 1. Of these kinases, aurA and aurB were inhibited by **NDPC4** and to verify this effect, the phosphorylation status of both kinases was determined using western blot analysis. Aurora kinase activity is accompanied by an increase in its phosphorylation [20]. Treatment with **NDPC4** decreased the phosphorylation of aurA, aurB, and aurC on threonine-288, -232, and -198, respectively (Figure 5A), as well as that of histone H3, a substrate of aurA and aurB, at serine 10 (Figure 5B) in a time-dependent fashion [21]. These data suggest that decreased phosphorylation of aurora kinases induced by **NDPC4** inhibited their kinase activity.

3.5. Molecular binding modes between NDPC4 and aurA and aurB

To evaluate the molecular binding mode between the aurora kinases and **NDPC4**, the *in silico* docking experiments were chosen. The 3D structure of **NDPC4** was generated using energy minimization based on the 3D structure of *N*,3,5-triphenyl-pyrazoline-1-carbothioamide (Suppl.

Figure 1) provided by the NCBI (PubChem CID: 3794935). The procedure used to determine the energy minimization was based on a previously reported method [11]. The 3D structure of aurA was obtained from the crystallographic structure of the complex of aurA and a ligand, 4-(4-methylpiperazin-1-yl)-N-[5-(2-thienylacetyl)-1,5-dihydropyrrolo[3,4-C]pyrazol-3-yl]benzamide (named 626) [Suppl. Figure 8], which was deposited in the PDB as 2J4Z.pdb. More than 100 3D structures of aurA can be found in the PDB, but 2J4Z.pdb contains most residues (126−395). The 2J4Z.pdb consists of two polypeptide chains, A and B, and chain B includes more residues than A. Therefore, 2J4Z-B was chosen for the *in silico* docking experiment. First, apoprotein was prepared using the Sybyl program. After its energy minimization, the root-mean-square deviation between the crystallographic structure and the energy-minimized structure was 0.30 Å. Since we used a flexible docking method, the docking radius was set to 6.5 Å. The docking process was repeated 30 times to generate 30 complexes. The substrate binding sites were determined based on the interpretation of the LigPlot analysis [22] [Suppl. Figure 9A]. Fifteen residues were used included in the binding site. When the original ligand, 626 was docked into the apoprotein, the binding energy ranged from -24.25 to -27.32 kcal/mol·Å. Similarly, **NDPC4** was docked into the apoprotein, and 30 complexes of aurA and **NDPC4** were obtained. Their binding energy ranged between -22.24 and -24.85 kcal/mol·Å. The first complex showed the best binding pose and lowest binding energy and, therefore, it was further analyzed. The LigPlot analysis revealed that 10 residues participated in the hydrophobic interactions between the apoprotein and **NDPC4**, and two residues formed four hydrogen bonds (H-bonds) [Suppl. Figure 9B]. Eight residues consisting of Agr137, Leu139, Ala160, Tyr212, Ala213, Pro214, Thr217, and Leu263 were observed in both complexes while in the aurA-626 and aurA-**NDPC**4 complex, two residues each (Glu211 and Ala213, and Ala137 and Tyr212) formed two and four H-bonds, respectively. The 3D images generated using the PyMol program (PyMOL Molecular Graphics System, version 1.3, Schrödinger, LLC) demonstrated the presence of different H-bonds [Suppl. Figure 10]. The binding energy of the aurA-**NDPC4** and aurA-626 complexes could be matched. Furthermore, even a lower number of residues in the aurA-**NDPC4** complex participated in the binding site than participated in that of the aurA-626 complex. Therefore, the four H-bonds of the aurA-**NDPC4** complex may have created a stronger interaction than the two H-bonds of the

aurA-626 complex did.

Similarly, the binding mode between **NDPC4** and aurB was elucidated using *in silico* docking. Because only one 3D structure of aurB was deposited in the PDB as 4AF3.pdb, it was chosen for the in silico docking. It contains a ligand, cyclopropanecarboxylic acid {4-[4-(4-methyl- piperazin-1-yl)-6-(5-methyl-2*h*-pyrazol-3-ylamino)-pyrimidin-2-ylsulfanyl]-phenyl}-amide (named VX6) [Suppl. Figure 11]. The binding energy of VX6 docked into the apo-aurB ranged from -24.43 to -29.87 kcal/mol·Å. The residues participating in the binding site were analyzed using LigPlot [Suppl. Figure 12A]. Eleven residues were found in the binding site of VX, and nine of them showed hydrophobic interactions while two formed three H-bonds. The docking process was applied to **NDPC4,** and the binding energy of the aurB-**NDPC4** complex ranged between -24.93 and -29.88 kcal/mol·Å. Furthermore, 14 residues were observed in the binding site analyzed using LigPlot [Suppl. Figure 12B] and one (Glu161) formed an H-bond while eight residues consisting of Leu83, Val91, Ala104, Glu155, Tyr156, Ala157, Gly160, and Leu207 were observed in both binding sites. The 3D images of the aurB-VX6 and aurB-**NDPC4** complex were generated using PyMol [Suppl. Figure 13]. In the aurB-**NDPC4** and aurB-VX6 complexes, 14 and 11 residues participated in the binding site. However, the aurB-**NDPC4** complex included one H-bond while the aurB-VX6 complex had three. This phenomenon may be responsible for the similar binding energy observed between the aurB-**NDPC4** and aurB-VX6 complexes. In order to develop NDPC derivatives for clinical cancer therapy, further rigorous studies are needed to determine the *in vivo* bioavailability and safety of the NDPC derivatives, including the pharmacokinetics (e.g. absorption, distribution, metabolism, and excretion) and toxicokinetic properties (e.g. acute toxicity and repeated-dose toxicity).

4. Conclusion

The cytotoxicities of most natural chalcones against HCT116 human colorectal cancer cells are evident at micromolar levels [23,24]. The NDPC derivatives investigated are derived chalcones, and their cytotoxicities ranged between 210 and 4788 nM. Therefore, a substitution of the α,β-unsaturated carbonyl group of chalcone with a pyrazoline group improved the cellular cytotoxicities. Furthermore, the 36 derivatives evaluated here possess the same skeleton, but the number and position of methoxy groups vary. To elucidate the relationships between their

cytotoxicities and the number and position of the methoxy groups, CoMFA and CoMSIA were used, and the analysis of their contour maps revealed that the C2 position favors hydrophobic and less bulky group while the other positions of the A ring are less involved in the cell growth inhibition. On the other hand, the inhibitory activity was affected by a combination of substituents on the B ring. It is possible that altering the 3D structure of the NDPC compounds with different substituents on B ring induced differential effects on the target protein. Therefore, we first sought to identify the target protein for **NDPC4**, which exhibited the best activity in the long-term survival clonogenic assay, using *in vitro* kinases assays with 17 kinases that are known to participate in the cell cycle. Because aurA and aurB were inhibited by **NDPC4**, we verified if this effect was mediated by the alteration of the phosphorylation status of the aurora kinases using western blot analysis. The result revealed that **NDPC4** decreased the phosphorylation of the aurora kinases by inhibiting their kinase activity. To evaluate the molecular binding mode between the aurora kinases and **NDPC4**, the *in silico* docking experiments were carried out. The binding energy of the aurA and **NDPC4** complex was matched with that of the aurA and ligand 626 contained in the aurA complex. Similarly, the binding energy between the aurB and **NDPC4** complex competed with that between the aurB and ligand VX6 contained in the aurB complex. Next, we evaluated the biological activities of **NDPC4**, which induced apoptosis and triggered cell death by apoptosis in HCT116 cells by a caspase-dependent mechanism. These findings could be used for the further development of NDPC derivatives as potential chemotherapeutic agents.

Acknowledgments

This work was supported by the Priority Research Centers Program (NRF, 2009-0093824) and Cooperative Research Program for Agriculture Science & Technology Development (RDA, PJ01130302). SY Shin was supported by the KU Research Professor Program of Konkuk University.

5. References

[1] N. Siddiqui, P. Alam, W. Ahsan, Arch Pharm (Weinheim). 342 (2009) 173-181.

[2] B. Kocyigit-Kaymakcioglu, N. Beyhan, N. Tabanca, A. Ali, D.E. Wedge, S.O. Duke, U.R. Bernier, I.A. Khan, Med Chem Res. 24 (2015) 3632-3644.

[3] S.Y. Shin, H. Yoon, D. Hwang, S. Ahn, D.W. Kim, D. Koh, Y.H. Lee, Y. Lim, Bioorg Med Chem. 21 (2013) 7018-7024.

[4] X. Wen, T. Walle, Drug Metab Dispos. 34 (2006) 1786-1792.

[5] J.R. Araujo, P. Goncalves, F. Martel, Nutr Res. 31 (2011) 77-87.

[6] N.A. Franken, H.M. Rodermond, J. Stap, J. Haveman, C. van Bree, Nat Protoc. 1 (2006) 2315-2319.

[7] H. Jung, S. Ahn, M. Park, H. Yoon, H.J. Noh, S.Y. Kim, J.S. Yoo, D. Koh, Y. Lim, Magn Reson Chem. 53 (2015) 383-390.

[8] H. Jung, S. Ahn, Y. Jung, H.J. Noh, S.Y. Kim, D. Koh, Y. Lim, Magn Reson Chem. 53 (2015) 391-397.

[9] S.Y. Shin, H. Jung, S. Ahn, D. Hwang, H. Yoon, J. Hyun, Y. Yong, H.J. Cho, D. Koh, Y.H. Lee, Y. Lim, Bioorg Med Chem. 22 (2014) 1809-1820.

[10] H. Yoon, T.W. Kim, S.Y. Shin, M.J. Park, Y. Yong, D.W. Kim, T. Islam, Y.H. Lee, K.Y. Jung, Y. Lim, Bioorg Med Chem Lett. 23 (2013) 232-238.

[11] J. Hyun, S.Y. Shin, K.M. So, Y.H. Lee, Y. Lim, Bioorg Med Chem Lett. 22 (2012) 2664-2669.

[12] S.Y. Shin, J.M. Lee, M.S. Lee, D. Koh, H. Jung, Y. Lim, Y.H. Lee, Clin Cancer Res. 20 (2014) 4302-4313.

[13] Y. Jung, S.Y. Shin, Y. Yong, H. Jung, S. Ahn, Y.H. Lee, Y. Lim, Chem Biol Drug Des. 85 (2015) 574-585.

[14] S.Y. Shin, H. Yoon, S. Ahn, D.W. Kim, S.H. Kim, D. Koh, Y.H. Lee, Y. Lim, Bioorg Med Chem. 21 (2013) 4250-4258.

[15] D. Fancelli, J. Moll, M. Varasi, R. Bravo, R. Artico, D. Berta, S. Bindi, A. Cameron, I. Candiani, P. Cappella, P. Carpinelli, W. Croci, B. Forte, M.L. Giorgini, J. Klapwijk, A. Marsiglio, E. Pesenti, M. Rocchetti, F. Roletto, D. Severino, C. Soncini, P. Storici, R. Tonani, P. Zugnoni, P. Vianello, J Med Chem. 49 (2006) 7247-7251.

[16] J.M. Elkins, S. Santaguida, A. Musacchio, S. Knapp, J Med Chem. 55 (2012) 7841-7848.

[17] J.J. Lum, D.E. Bauer, M. Kong, M.H. Harris, C. Li, T. Lindsten, C.B. Thompson, Cell. 120 (2005) 237-248.

[18] H.A. Andree, C.P. Reutelingsperger, R. Hauptmann, H.C. Hemker, W.T. Hermens, G.M. Willems, J Biol Chem. 265 (1990) 4923-4928.

[19] D.R. McIlwain, T. Berger, T.W. Mak, Cold Spring Harb Perspect Biol. 5 (2013) a008656.

[20] A.O. Walter, W. Seghezzi, W. Korver, J. Sheung, E. Lees, Oncogene. 19 (2000) 4906-4916.

[21] C. Crosio, G.M. Fimia, R. Loury, M. Kimura, Y. Okano, H. Zhou, S. Sen, C.D. Allis, P. Sassone-Corsi, Mol Cell Biol. 22 (2002) 874-885.

[22] A.C. Wallace, R.A. Laskowski, J.M. Thornton, Protein Eng. 8 (1995) 127-134.

[23] D.H. Lee, Y.J. Jung, D. Koh, Y. Lim, Y.H. Lee, S.Y. Shin, Cancer Lett. 372 (2016) 1-9.

[24] J.M. Lee, M.S. Lee, D. Koh, Y.H. Lee, Y. Lim, S.Y. Shin, Cancer Lett. 354 (2014) 348-354.

Figure legends

Figure 1. Structures of (A) diphenylpyrazoline-1-carbothioamide, (B) 3-naphthalen-2-yl-5-methoxyphenyl-pyrazoline-1-carbothioamide, (C) 3-(naphthalen-2-yl)-*N*,5-dimethoxyphenyl-pyrazoline-1-carbothioamide, and (D) 3-(1-hydroxynaphthalen-2-yl)-*N*,5-dimethoxyphenyl-pyrazoline-1-carbothioamide.

Figure 2. Clonogenic long-term survival assays of 36 3-(naphthalen-2-yl)-*N*,5-diphenyl-pyrazoline-1-carbothioamide (NDPC) derivatives at four different concentrations (0, 50, 500, and 5000 nM).

Figure 3. Antiproliferative effect of 3-(naphthalen-2-yl)-*N*,5-diphenyl-pyrazoline-1-carbothioamide (**NDPC**)-**4** in HCT116 cells. (A) Cell viability test using cell counting kit-8 (CCK-8). HCT116 cells (1×10^3 cells/sample) were treated with different concentrations of NDPC4 (0, 5, 10, 20, and 40 μM) for 24 h. (B) Effect of **NDPC4** on cell cycle distribution. Cells were treated with 10 μM **NDPC4** for 24 h, fixed with ethanol, and stained with propidium iodide (PI). Cellular DNA content was determined using flow cytometry using a NucleoCounter NC-3000; *x*-axis, cell counts; *y*-axis, PI-stained DNA contents; 2N, diploid; 4N, tetraploid. (C) Effect of **NDPC4** on expression of cyclin D1 and cyclin B1. Cells were treated with 10 μM **NDPC4** for 0, 3, 6, 12, and 24 h. Whole-cell lysates were prepared and subjected to western blotting. Glyceraldehyde 3-phosphate dehydrogenase (GAPDH) was the internal control used to ensure equal protein loading.

Figure 4. Effect of 3-(naphthalen-2-yl)-*N*,5-diphenyl-pyrazoline-1-carbothioamide (**NDPC**)-**4** on induction of apoptosis. HCT116 cells were treated with 20 μM **NDPC4** for 24 h and then stained with fluorescein isothiocyanate (FITC)-annexin-V and propidium iodide (PI). Cells were harvested, washed, and analyzed for fluorescence intensity using flow cytometer. (A) Scatter plots show the FITC-annexin V intensity versus that of PI. (B) Histograms show the FITC-annexin V intensity of the cell counts (%). (C) Cells were treated with 10 μM **NDPC4** for 0, 12, and 24 h. Whole-cell lysates were prepared and subjected to western blotting using antibodies

against cleaved caspase-7 and poly(adenosine diphosphate [ADP]-ribose) polymerase (PARP). Glyceraldehyde 3-phosphate dehydrogenase (GAPDH) antibody was the internal control used to show equal protein loading.

Figure 5. Effect of 3-(naphthalen-2-yl)-*N*,5-diphenyl-pyrazoline-1-carbothioamide (**NDPC**)-**4** on phosphorylation of aurora kinases in HCT116 cells treated with 20 μM **NDPC4** for various lengths of time. Whole cell lysates were prepared, and we analyzed phosphorylated levels of (A) aurora kinase A (aurA), aurB, and aurC on threonine-288,-232, and -198 and (B) histone H3 on serine-10 using western blotting. Glyceraldehyde 3-phosphate dehydrogenase (GAPDH) antibody was the internal control used to show equal protein loading.

Scheme 1. The synthetic procedures of 3-(naphthalen-2-yl)-*N*,5-diphenyl-pyrazoline-1-carbothioamide derivatives **1**-**36**.

Table 1. Structures and biological data of 36 synthesized 3-(naphthalen-2-yl)-*N*,5-diphenyl-pyrazoline-1-carbothioamide (NDPC) derivatives.

Suppl. Table 1. Experimental half-maximal cell growth inhibitory concentration negative logarithmic scale (pGI_{50}) data and pGI_{50} values predicted using comparative molecular field analysis (CoMFA) and comparative molecular similarity index analysis (CoMSIA) models.

Suppl. Figure 1. Structure of *N*,3,5-triphenyl-pyrazoline-1-carbothioamide.

Suppl. Figure 2. Clonogenic long-term survival assays of 36 3-(naphthalen-2-yl)-*N*,5-diphenyl-pyrazoline-1-carbothioamide (NDPC) derivatives at four different concentrations (0, 5, 10, and 20 μM).

Suppl. Figure 3. Hierarchical clustering tree; *indicates selective derivatives for the test set used for the quantitative structure-activity relationship (QSAR) calculation.

Suppl. Figure 4. Plot of experimental data versus values predicted using comparative molecular field analysis (CoMFA). Diamonds and squares denote training and test sets, respectively.

Suppl. Figure 5. Comparative molecular field analysis (CoMFA) contour maps. (A) Steric field contours are shown in green (more bulkiness favored) and yellow (less bulkiness favored). (B) Electrostatic field contours are shown in red (electronegative substituents favored) and blue (electropositive substituents favored).

Suppl. Figure 6. Plot of experimental data versus values predicted using comparative molecular similarity index analysis (CoMSIA). Diamonds and squares denote training and test sets, respectively.

Suppl. Figure 7. Comparative molecular similarity index analysis (CoMSIA) contour maps. (A) Steric field contours are shown in green (more bulkiness favored) and yellow (less bulkiness favored). (B) Electrostatic field contours are shown in red (electronegative substituents favored) and blue (electropositive substituents favored). (C) Hydrophobic field contours are shown in orange (hydrophobic favored) and white (hydrophobic disfavored). (D) H-bond acceptor filed

contours are shown in magenta (H-bond acceptor favored) and cyan (H-bond acceptor disfavored).

Suppl. Figure 8. Structure of 4-(4-methylpiperazin-1-yl)-*N*-[5-(2-thienylacetyl)-1,5-dihydropyrrolo[3,4-C]pyrazol-3-yl]benzamide (named 626) contained in 2J4Z.pdb as a ligand.

Suppl. Figure 9. Residues participating in binding sites of (A) aurora kinase A (aurA)-626 and (B) aurA-3-(naphthalen-2-yl)-*N*,5-diphenyl-pyrazoline-1-carbothioamid (**NDPC**)-**4** complexes were analyzed using LigPlot program. Residues in half circles create hydrophobic interactions with the ligands, and dotted lines denote H-bonds.

Suppl. Figure 10. Three-dimensional (3D) images of binding sites of (A) aurora kinase A (aurA)-626 complex and (B) aurA-3-(naphthalen-2-yl)-*N*,5-diphenyl-pyrazoline-1-carbothioamid (**NDPC**)-**4** complex were generated using PyMOL program. Ligands 626 and **NDPC4** are shown in yellow and magenta, respectively. Cyan-colored lines represent H-bonds.

Suppl. Figure 11. Structure of cyclopropanecarboxylic acid {4-[4-(4-methyl- piperazin-1-yl)-6-(5-methyl-2*h*-pyrazol-3-ylamino)-pyrimidin-2-ylsulfanyl]-phenyl}-amide (named VX6) contained in 4AF3.pdb as a ligand.

Suppl. Figure 12. Residues participating in binding sites of (A) aurora kinase B (aurB)-VX6 complex and (B) aurB-3-(naphthalen-2-yl)-*N*,5-diphenyl-pyrazoline-1-carbothioamid (**NDPC**)-**4** complexes were analyzed using LigPlot program. Residues in half circles create hydrophobic interactions with ligands, and dotted lines denote H-bonds.

Suppl. Figure 13. Three-dimensional (3D) images of binding sites of (A) aurora kinase B (aurB)-VX6 and (B) aurB-3-(naphthalen-2-yl)-*N*,5-diphenyl-pyrazoline-1-carbothioamid (**NDPC**)-**4** complexes were generated using PyMOL program. Ligands VX6, and **NDPC4** are shown in yellow and magenta, respectively. Cyan-colored lines represent H-bonds.

Fig.1

(A)

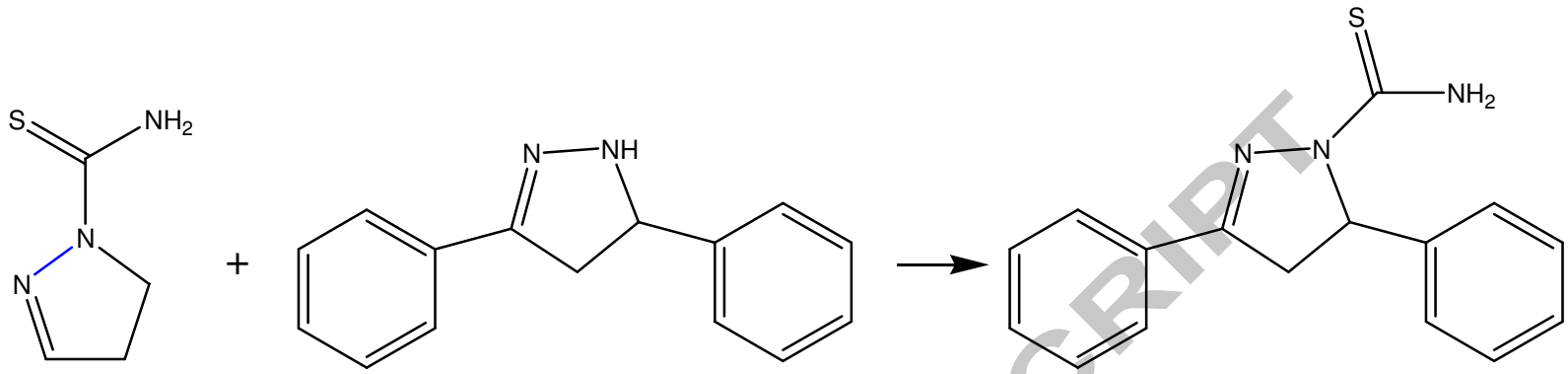

pyrazoline-1-carbothioamide diphenylpyrazoline diphenylpyrazoline-1-carbothioamide

(B)

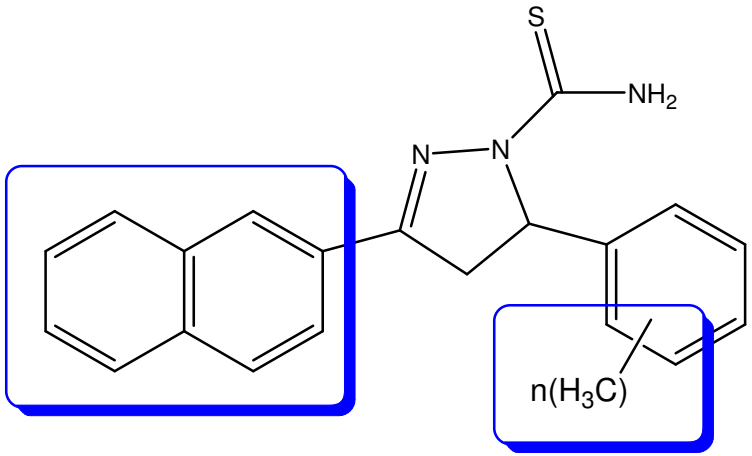

Fig.1

(C)

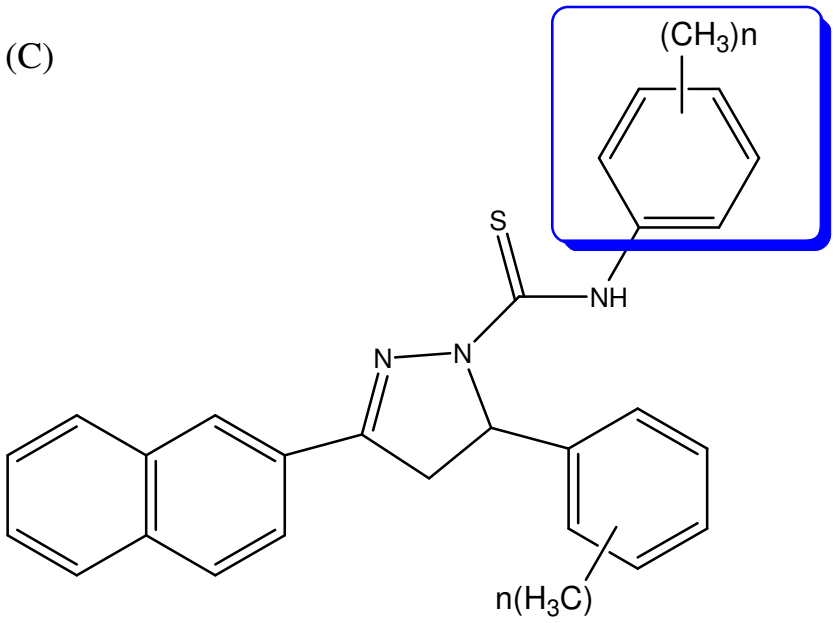

(D)

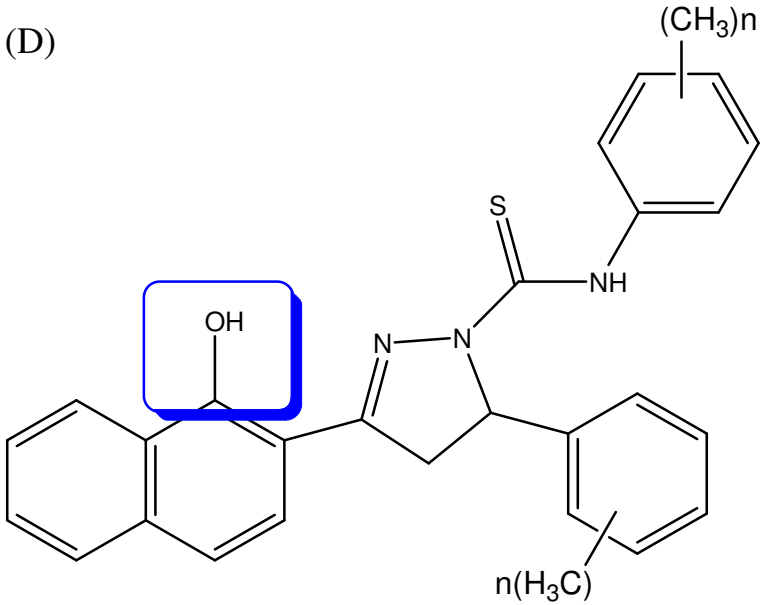

Fig.2

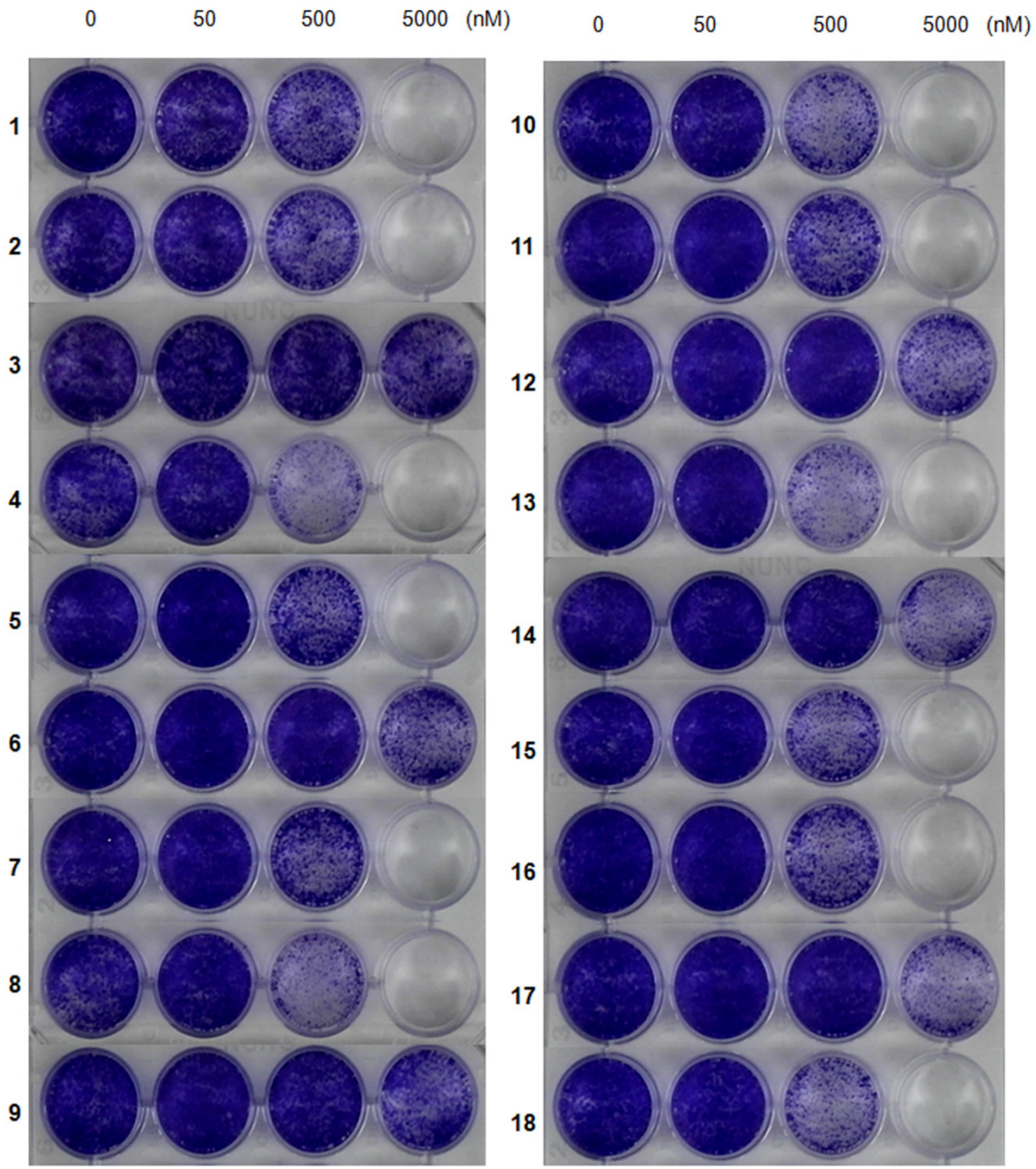

Fig.2

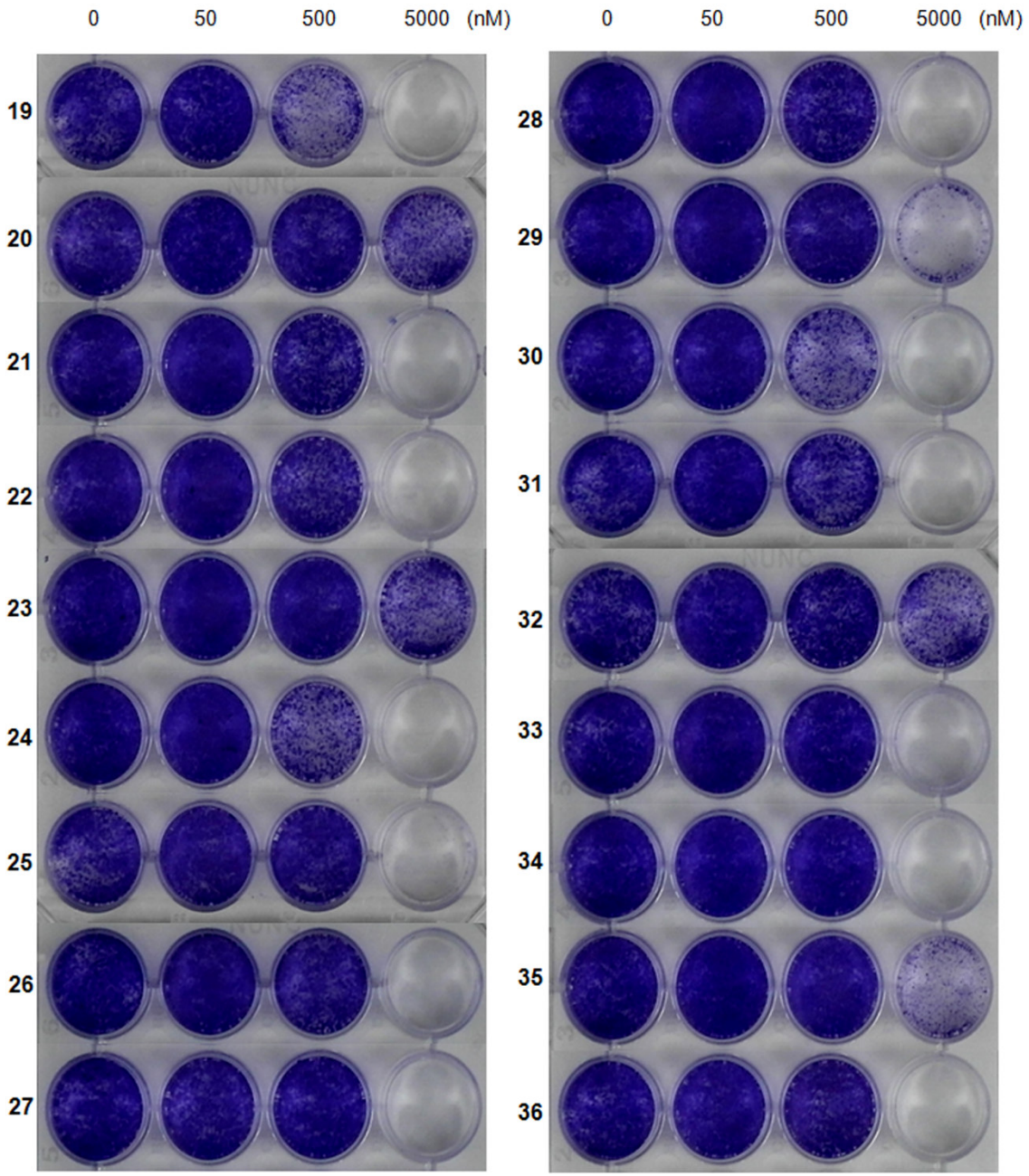

Fig.3

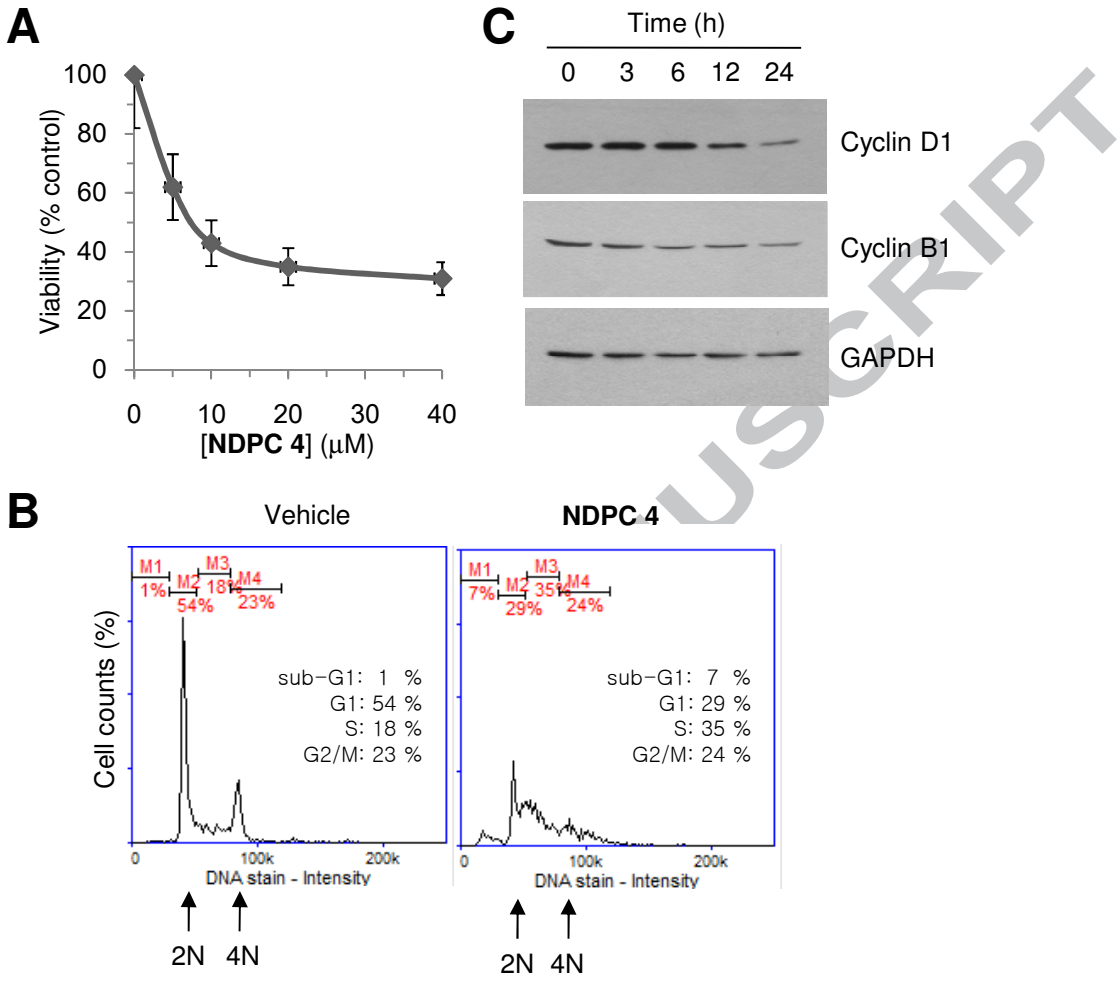

Fig.4

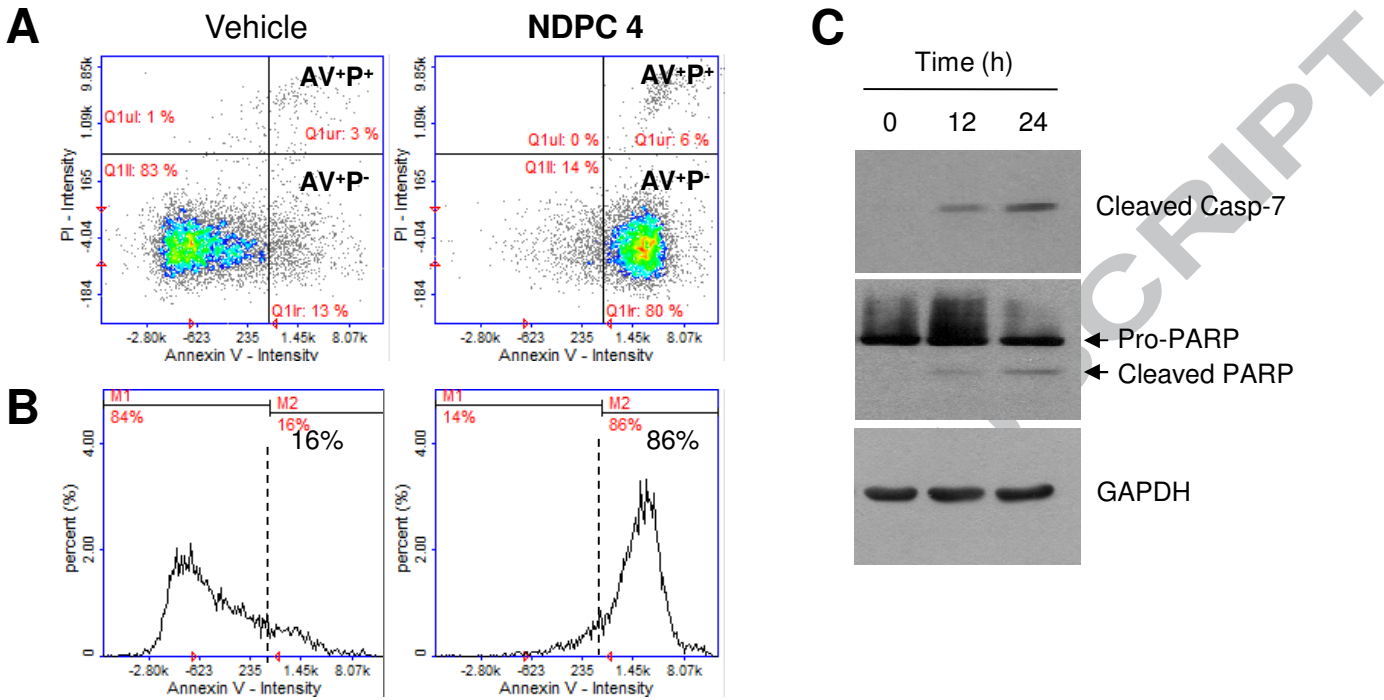

Fig.5

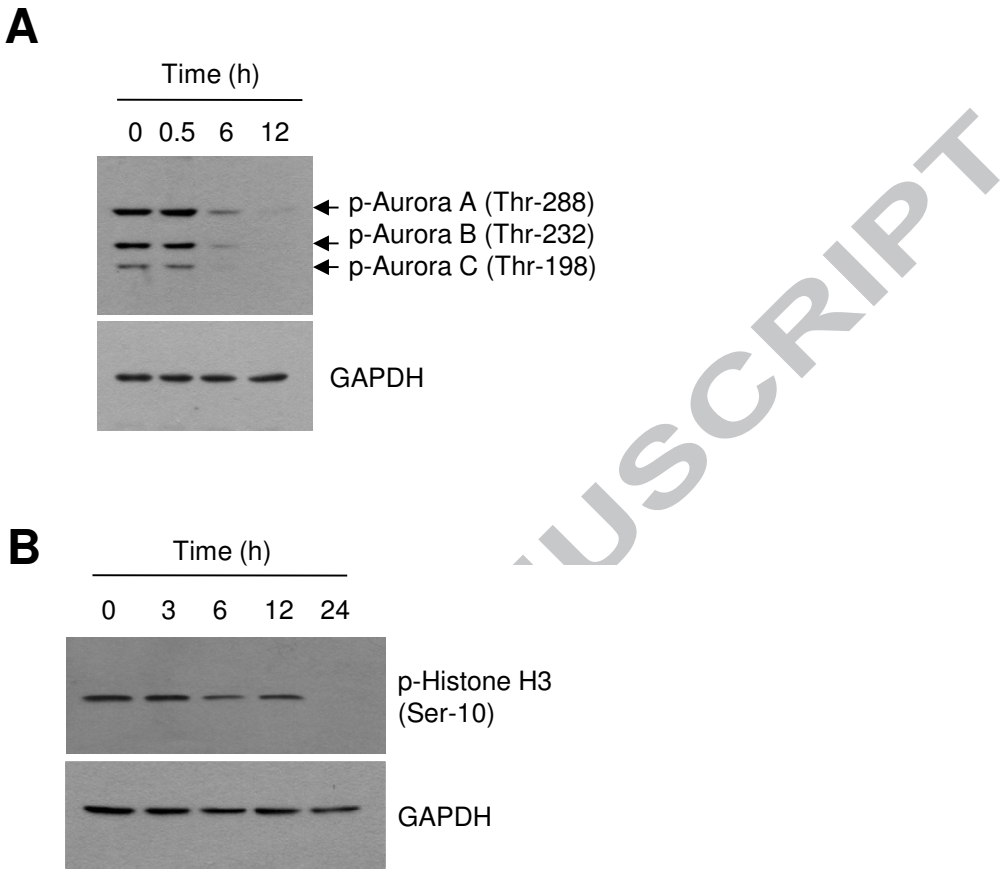

Scheme 1

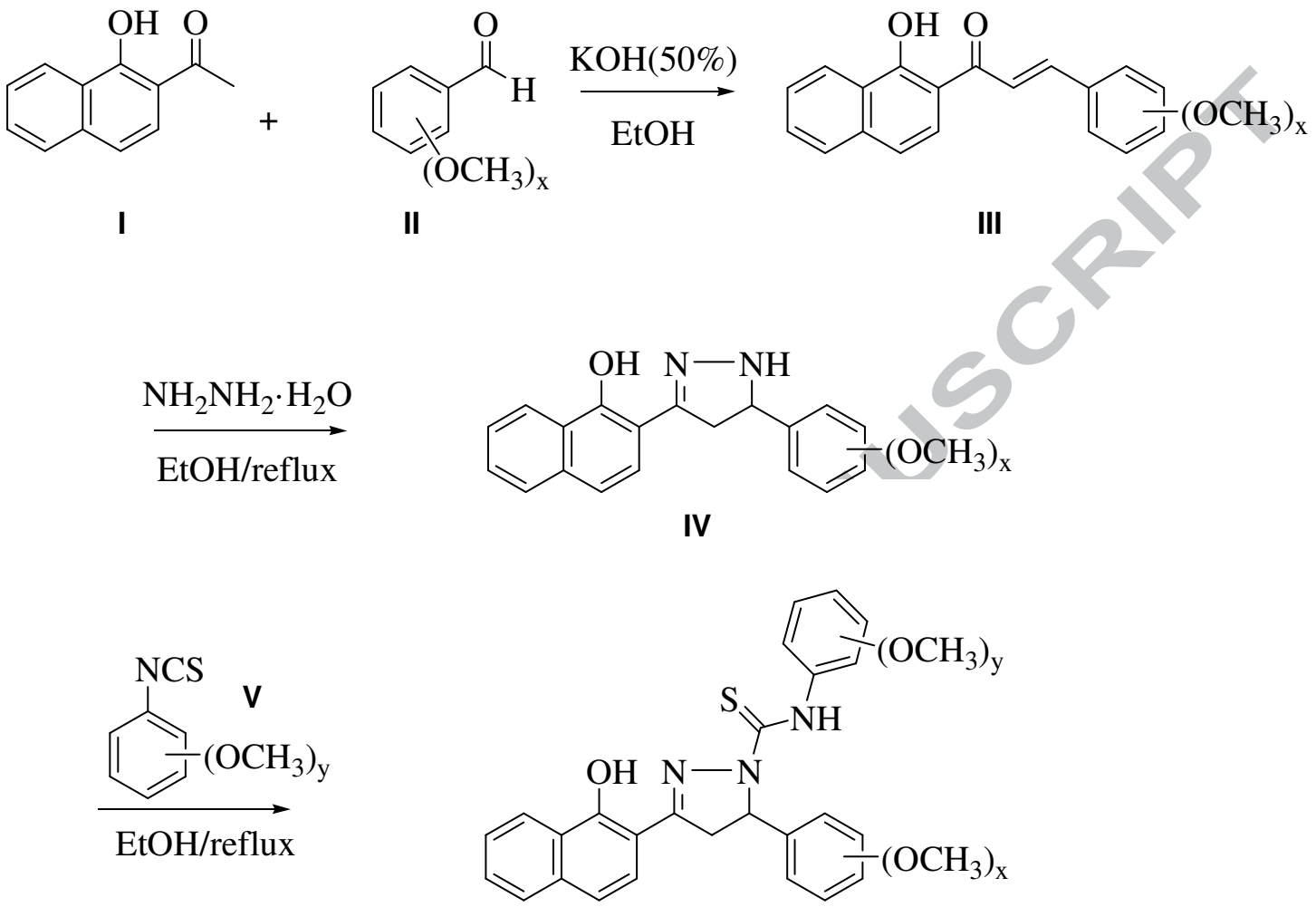

NDPC 1 - 36

Table 1. Structures and biological data of 36 synthesized 3-(naphthalen-2-yl)-*N*,5-diphenyl-pyrazoline-1-carbothioamide (NDPC) derivatives.

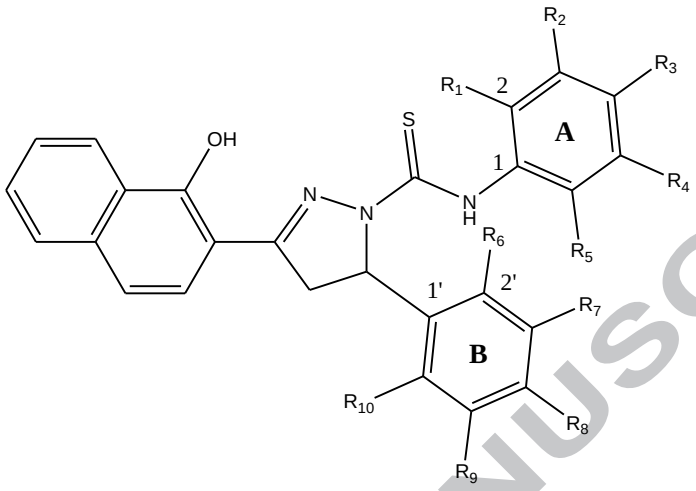

	R_1	R_2	R_3	R_4	R_5	R_6	R_7	R_8	R_9	R_{10}	IC_{50}(nM)	pIC_{50}
1	H	H	H	H	H	OCH_3	OCH_3	H	H	H	765.44	3.116
2	H	H	OCH_3	H	H	OCH_3	OCH_3	H	H	H	799.07	3.097
3	OCH_3	H	H	H	H	OCH_3	OCH_3	H	H	H	4788.65	2.320
4	H	H	H	H	H	H	OCH_3	H	OCH_3	H	210.552	3.677
5	H	OCH_3	H	H	H	OCH_3	OCH_3	H	H	H	1129.34	2.947
6	OCH_3	H	OCH_3	H	H	OCH_3	OCH_3	H	H	H	3836.60	2.416
7	H	OCH_3	OCH_3	OCH_3	H	OCH_3	OCH_3	H	H	H	705.29	3.152
8	H	H	H	H	H	OCH_3	H	OCH_3	H	H	391.11	3.408
9	OCH_3	H	H	H	H	OCH_3	H	OCH_3	H	H	4029.26	2.395
10	H	OCH_3	H	H	H	OCH_3	H	OCH_3	H	H	367.47	3.435
11	H	H	OCH_3	H	H	OCH_3	H	OCH_3	H	H	812.68	3.090
12	OCH_3	H	OCH_3	H	H	OCH_3	H	OCH_3	H	H	4064.38	2.391
13	H	OCH_3	OCH_3	OCH_3	H	OCH_3	H	OCH_3	H	H	305.51	3.515
14	OCH_3	H	H	H	H	H	OCH_3	H	OCH_3	H	3871.31	2.412
15	H	OCH_3	H	H	H	H	OCH_3	H	OCH_3	H	379.00	3.421
16	H	H	OCH_3	H	H	H	OCH_3	H	OCH_3	H	463.47	3.334
17	OCH_3	H	OCH_3	H	H	H	OCH_3	H	OCH_3	H	2640.82	2.578
18	H	OCH_3	OCH_3	OCH_3	H	H	OCH_3	H	OCH_3	H	311.77	3.506
19	H	H	H	H	H	OCH_3	OCH_3	OCH_3	H	H	444.33	3.352
20	OCH_3	H	H	H	H	OCH_3	OCH_3	OCH_3	H	H	4763.82	2.322
21	H	OCH_3	H	H	H	OCH_3	OCH_3	OCH_3	H	H	2074.85	2.683
22	H	H	OCH_3	H	H	OCH_3	OCH_3	OCH_3	H	H	2485.91	2.605
23	OCH_3	H	OCH_3	H	H	OCH_3	OCH_3	OCH_3	H	H	3917.76	2.407

24	H	OCH_3	OCH_3	OCH_3	H	OCH_3	OCH_3	OCH_3	H	H	494.93	3.305
25	H	H	H	H	H	OCH_3	H	OCH_3	OCH_3	H	2579.09	2.589
26	OCH_3	H	H	H	H	OCH_3	H	OCH_3	OCH_3	H	2536.33	2.596
27	H	OCH_3	H	H	H	OCH_3	H	OCH_3	OCH_3	H	2427.13	2.615
28	H	H	OCH_3	H	H	OCH_3	H	OCH_3	OCH_3	H	2296.94	2.639
29	OCH_3	H	OCH_3	H	H	OCH_3	H	OCH_3	OCH_3	H	2249.44	2.648
30	H	OCH_3	OCH_3	OCH_3	H	OCH_3	H	OCH_3	OCH_3	H	474.33	3.324
31	H	H	H	H	H	OCH_3	H	OCH_3	H	OCH_3	1938.25	2.713
32	OCH_3	H	H	H	H	OCH_3	H	OCH_3	H	OCH_3	4374.14	2.359
33	H	OCH_3	H	H	H	OCH_3	H	OCH_3	H	OCH_3	2558.53	2.592
34	H	H	OCH_3	H	H	OCH_3	H	OCH_3	H	OCH_3	2529.11	2.597
35	OCH_3	H	OCH_3	H	H	OCH_3	H	OCH_3	H	OCH_3	1901.85	2.721
36	H	OCH_3	OCH_3	OCH_3	H	OCH_3	H	OCH_3	H	OCH_3	2602.44	2.585

Graphical abstract

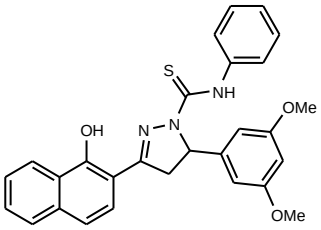

3-(1-hydroxynaphthalen-2-yl)-5-(3,5-dimethoxyphenyl)-*N*-phenyl-pyrazoline-1-carbothioamide (**NDPC4**)

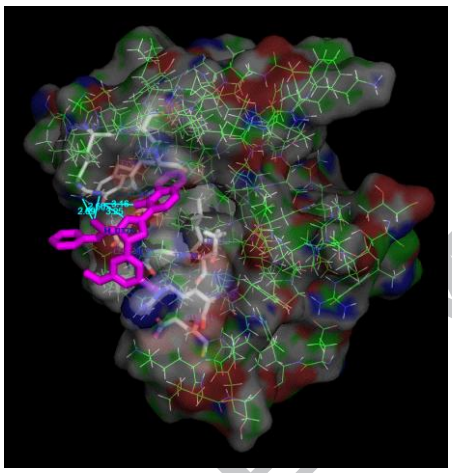

aurora A – NDPC4 complex

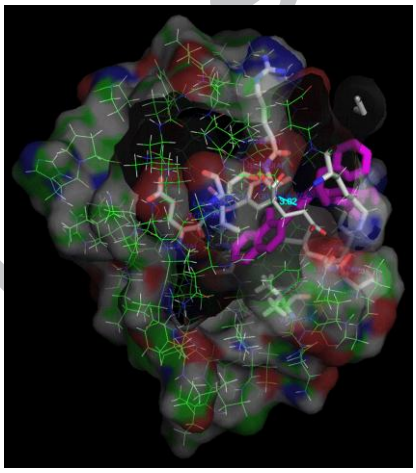

aurora B – NDPC4 complex

Highlights

- *Compounds with 3-(naphthalen-2-yl)-N,5-diphenyl-pyrazoline-1-carbothioamide skeletons were synthesized.*
- *Their GI_{50} ranged from a few hundred nM to a few μM.*
- *Aurora kinases A and B were inhibited by the title compound.*
- *In silico docking study between the title compound and aurora kinases A and B was performed.*
- *The structural conditions required for good cytotoxicity were identified*